

Computational prediction and experimental confirmation of B-site doping in YBa₂Fe₃O₈

Christopher Collins¹, Matthew S Dyer¹, Antoine Demont¹, Philip A Chater¹, Michael F Thomas², George R Darling¹, John B Claridge¹, Matthew J Rosseinsky¹

¹Department of Chemistry, University of Liverpool, Crown Street, Liverpool, L69 7ZD, UK.

²Department of Physics, University of Liverpool, Liverpool, L69 7ZE, UK.

Electronic Supplementary Information

Computational methods

Calculations were performed using the plane wave density functional theory (DFT) package, Vienna Ab-initio Simulation Package (VASP) version 4.6.26^{64, 65} with the Perdew, Burke and Ernzerhof (PBE)⁶⁶ exchange correlation functional. For the B-site species (Fe, Co, Mn and Ni) the first sub-valence p-orbitals were treated as valence and for the A-site species (Y and Ba) the first sub-valence s-orbital was treated as valence. The *k*-point grid that was used for each calculation was determined by the first gamma centred *k*-point grid that fulfilled the condition:

$$nk_i \times r_i \geq 20 \text{ \AA} \quad (S1)$$

where nk_i is the number of *k*-points on lattice vector *i* and r_i is the length of the corresponding real lattice vector, given in Å. The unit cell size, shape and atomic coordinates were relaxed until forces on atoms were less than 0.01 eV/Å. Wavefunctions were converged until the difference in energy between consecutive steps was less than 10⁻⁵ eV. The plane wave cut-off energy in these calculations was set to 450 eV.

Collinear spin-polarization was applied to the B-sites for YBa₂Fe_{3-x}M_xO₈ as follows without spin-orbit coupling: when $x = 0$ or $M = \text{Co}$ a G-type antiferromagnetic structure was used, as reported for YBa₂Fe₃O₈; for $M = \text{Ni}$ and Mn , both G-type antiferromagnetic and ferromagnetic arrangements were tested. Collinear magnetic structures were also applied to the binary oxide calculations in arrangements that have been experimentally reported^{42-44, 47}.

It has been shown that in order to be able to calculate accurate formation energies for perovskites containing d electrons, an onsite Coulomb interaction term, *U*, must be applied to the d-orbitals of the transition metals⁴¹. We have followed the approach of Dudarev et al.⁶⁷, using an effective U_{eff} where $U_{\text{eff}} = U - J$. In this work we used values of U_{eff} of 4.0, 4.0, 6.4 and 3.3 eV for Fe, Mn, Ni and Co respectively, values chosen to reproduce experimental energies for the oxidation of binary oxides⁴¹. The energy of O₂ gas was fixed as -8.5 eV per formula unit (FU), a value which includes a correction to the DFT calculated binding energy of O₂ obtained by fitting to the experimental formation energies of binary oxides⁴¹.

The expected extent of ordering at finite temperatures based on 0 K DFT energies, was modelled using a statistical mechanics approach detailed in the literature³⁰. This approach estimates the occupation of different configurations at finite temperatures using Boltzmann statistics based upon the calculated enthalpy differences between configurations at 0 K and their configurational

entropies. For temperatures well below the Néel temperature (~ 700 K), the enthalpy differences between configurations calculated with G-type antiferromagnetic ordering are used. At higher temperatures, the mean of the enthalpy differences using G-type antiferromagnetic and ferromagnetic ordering is used to model paramagnetism.

Free energies of reaction were calculated according to the reaction schemes outlined in Equation 2, yielding a free energy of reaction, labelled ΔF_{sub} . The free energy of O_2 in the gas phase is approximated to be $-8.5 \text{ eV/FU} - k_B T \ln(p_{O_2})$, where p_{O_2} indicates the partial pressure of oxygen gas. All of the binary oxides and the undoped $YBa_2Fe_3O_8$ are assumed to be fully ordered and therefore have zero configurational entropy. The free energy of the doped compositions was calculated as outlined previously³⁰. For each of the doped $3a_p$ compounds, the free energy is calculated according to

$$F = -k_B T \ln Z \quad (S2)$$

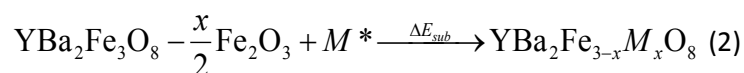
where the partition function, Z , is defined as

$$Z = \sum_{m=1}^N \Omega_m \exp\left(\frac{-E_m}{k_B T}\right) \quad (S3)$$

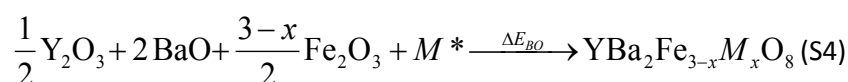
N indicates the total number of configurations, m , which include different magnetic orderings where calculated. E_m is the 0 K energy and Ω_m the degeneracy of configuration m . The degeneracy is given by the number of equivalent ways that the configuration can be modelled within the supercell. Vibrational contributions to the free energy were neglected, given the similarity between the structures on either side of Equation 2, and the considerable extra computational expense required to accurately calculate these contributions. Free energies were calculated at the synthesis temperature, 1473 K, and at partial pressures corresponding to air ($p_{O_2} = 0.21$) and pure O_2 ($p_{O_2} = 1$) at atmospheric pressure.

Related Reaction Energies

We define a substitution energy, ΔE_{sub} , using Equation 2:



Alternatively a reaction energy of formation for the doped and undoped compounds from binary oxides, ΔE_{BO} , can be calculated:



We note that the value of ΔE_{BO} differs from that of ΔE_{sub} only by a constant given by the formation energy of $YBa_2Fe_3O_8$ from binary oxides. ΔE_{BO} could therefore be used interchangeably with ΔE_{sub} with the sole result of shifting the energies by a constant value of 1.57 eV/Formula Unit.

Experimental methods

Samples were synthesised from binary oxides and carbonates (Y_2O_3 (99.999%), BaCO_3 (99.997%), Fe_2O_3 (99.998%), MnO_2 (99.97%), NiO (99.998%) purchased from Alfa Aesar and subsequently pre-dried) and weighed out in stoichiometric quantities. Samples were hand-ground using a pestle and mortar with the samples under acetone. Prior to firing the samples were pelletized using a uniaxial press at a pressure of approximately 5 tons, with the diameter of the pellet chosen to allow for the pellet to be < 5 mm thick. Samples were then heated at a temperature of 1200°C in a tube furnace under flowing N_2 (static air was also trialled for $\text{YBa}_2\text{FeNi}_2\text{O}_{8\pm\delta}$ and $\text{YBaFe}_2\text{MnO}_{8\pm\delta}$ materials) for 72 hours in alumina crucibles, with intermediate re-grinding and re-pelletisation at 24 and 48 hours. At the end of each heating cycle the samples were allowed to cool completely to room temperature before the gas flow was removed. Initial samples were synthesised with a target mass of 1 g. A larger sample was synthesised with a target mass of 7 g for NPD using the same methodology as above under flowing N_2 gas, as a single 32 mm diameter pellet.

Iodometric titrations were carried out in order to determine the oxygen content and therefore average transition metal charge state. Samples were titrated against sodium thiosulfate solution (0.1 M), standardised against potassium iodate (99.995% purchased from Sigma Aldrich). Samples of Fe_2O_3 and MnO_2 (purity and supplier as used in the synthesis) were also titrated and analysed to test the titration conditions for the transition metals in question, resulting in oxygen contents of $\text{O}_{3.00(3)}$ and $\text{O}_{2.01(2)}$ respectively.

For the titrations, an approximate ratio of 1 g of potassium iodide (99.99%, purchased from Alfa Aesar) was added for every 50 mg of sample. The potassium iodate standard was dissolved in water (ca. 20 cm^3) and then sulphuric acid added (ca. 5 cm^3 , 1 M). Metal oxides were dissolved in hydrochloric acid (20 cm^3 , 3 M), flushed with argon gas for at least 1 minute, sealed with laboratory film and stirred just above room temperature until samples were dissolved. The metal oxide samples were then diluted to an acid concentration of 0.5 M and titrated immediately. Samples were titrated until a pale straw colour was obtained, at which point, 2 cm^3 of starch indicator solution was added, turning the solution dark indigo, and the titration was continued to a clear end point. All titrations were repeated a minimum of 3 times and the average result is reported together with the standard error calculated from the spread of the results.

Mössbauer spectra at room temperature and at 77 K were taken in absorption mode with samples mounted between the Mössbauer source and the gamma ray detector. The source motion was controlled by a waveform that gave constant acceleration motion. A double ramp waveform was used so that the folded spectra have a flat background. The source was of ^{57}Co in a Rh matrix and the 14.4 keV gamma radiation was detected in a proportional counter filled with an argon/methane gas mixture to a pressure of about one atmosphere. The detector efficiency is about 67% for 14.4 keV radiation but is essentially zero for the 122 keV radiation that feeds the 14.4 keV state in ^{57}Fe . The spectrometer was calibrated against the known spectrum of α -iron (BCC). Values of isomer shift are quoted relative to α -iron at room temperature. The spectra are fitted with a superposition of components each of which represents a particular Fe ion in a defined environment. For each such component values of the isomer shift, electric quadrupole interaction and magnetic hyperfine field were determined.

All powder diffraction data were collected at room temperature. PXRD data were collected on the initial samples using a Bruker D8 Advance diffractometer using Cu $K\alpha_1$ ($\lambda = 1.5406 \text{ \AA}$) radiation in Bragg-Brentano or transmission foil geometry. For the structure refinement PXRD data was collected using a Bruker D8 Advance in Debye-Scherrer geometry using a 0.3 mm capillary with Mo $K\alpha_1$ ($\lambda = 0.7093 \text{ \AA}$) radiation (d -space range: 0.62 – 16.37 \AA), with backgrounds fitted with Chebyshev functions and 518 reflections calculated. Time Of Flight (TOF) - NPD patterns were collected at STFC-ISIS on the HRPD instrument in a 8 mm vanadium can, with data collected at 168° and 90° detector banks (with d -space ranges 0.67 – 2.36 and 0.96 – 3.67 \AA respectively) with backgrounds fitted using a power series with increasing Q (background type 4 in GSAS) with 669 and 437 reflections calculated for the 168° and 90° banks respectively. For phase identification X'Pert Highscore Plus software⁶⁸ was used to perform peak assignments using the pdf-2 database⁶⁹. Phase fractions quoted in Figure 6 were calculated using the computer program Topas Academic^{70, 71}. Rietveld refinements were performed using the GSAS^{72, 73} package, following a refinement method based upon a previously reported procedure on refining the nuclear and magnetic structure of $\text{YBa}_2\text{Fe}_3\text{O}_8$ ⁵⁴.

During the refinement process, both of the magnetic structures reported for orthorhombic $\text{YBa}_2\text{Fe}_3\text{O}_8$ ^{21, 54} were trialled with a fixed, previously refined nuclear structure and thus fixed unit cell parameters for the magnetic cells. This results in 5 re-finable parameters for both models; the scale parameter for each diffraction pattern (three parameters) and the magnitude of the magnetic moment on the square pyramidal and octahedral sites (two parameters).

When the magnetic structure was refined with the monoclinic cell ($P2'/m$ spacegroup²¹) the unit cell parameters were $a = b = 5.490923 \text{ \AA}$, $c = 23.968430$, $\alpha = \beta = 90^\circ$ and $\gamma = 90.042^\circ$. The symmetry and setting of the space group restrain the magnetic moments to lie along the **b** axis of the magnetic cell, in between the **a** and **b** axis of the nuclear unit cell, resulting in the magnetic moments aligned between the M-O bonds. The magnetic moments were refined to 3.57(5) μ_B on the octahedral site and 3.07(2) μ_B on the square pyramidal site, with the fit resulting in a χ^2 equal to 4.54.

When the magnetic structure was refined in the orthorhombic unit cell ($Fmm'm'$ spacegroup⁵⁴) the unit cell parameters were $a = 7.768143 \text{ \AA}$, $b = 7.762479 \text{ \AA}$, $c = 23.968430 \text{ \AA}$ and $\alpha = \beta = \gamma = 90^\circ$ (**a** = 2**a**, **b** = 2**b** and **c** = 2**c** relative to the nuclear cell). The magnetic moments are constrained by symmetry to lie along the **a** axis of the magnetic cell, which is in inline with the M-O bonds in the nuclear unit cell. The magnetic moments were refined to be 2.81(4) μ_B and 3.41(2) μ_B on the octahedral and square pyramidal sites respectively, the fit resulted in a χ^2 equal to 4.44. Since the $Fmm'm'$ magnetic cell had a slightly lower χ^2 compared to the $P2'/m$ model and it retains the orthorhombic unit cell type of the nuclear structure, it was used in the final refinement presented in the main text.

During the refinement, it was also possible to determine which of the **a** or **b** axis the magnetic moments were aligned along in the $Fmm'm'$ magnetic cell, by repeating the same as refinement above, with the **a** and **b** axes switched so that the magnetic cell becomes **a** = 2**b**, **b** = 2**a** and **c** = 2**c** relative to the nuclear unit cell, which results in a higher χ^2 , equal to 4.71 and magnetic moments of 2.77(4) μ_B and 3.38(2) μ_B on the octahedral and square pyramidal sites respectively, with the calculated patterns characterised by magnetic only reflections being calculated at incorrect Q values, confirming that the magnetic moments align along the **a** axis of the nuclear structure.

References

1. M. A. Pena and J. L. G. Fierro, *Chem. Rev.*, 2001, **101**, 1981-2017.
2. A. Aguadero, L. Fawcett, S. Taub, R. Woolley, K. T. Wu, N. Xu, J. A. Kilner and S. J. Skinner, *J. Mater. Sci.*, 2012, **47**, 3925-3948.
3. T. Minami, *Semicond. Sci. Technol.*, 2005, **20**, S35-S44.
4. J. P. Attfield, *J. Mater. Chem.*, 2011, **21**, 4756-4764.
5. V. V. Shvartsman and D. C. Lupascu, *J. Am. Ceram. Soc.*, 2012, **95**, 1-26.
6. L. B. Kong, S. Li, T. S. Zhang, J. W. Zhai, F. Y. C. Boey and J. Ma, *Prog. Mater. Sci.*, 2010, **55**, 840-893.
7. J. W. Fergus, *J. Eur. Ceram. Soc.*, 2012, **32**, 525-540.
8. Y. L. Chen and S. F. Yang, *Adv. Appl. Ceram.*, 2011, **110**, 257-269.
9. R. C. Pullar, *Prog. Mater. Sci.*, 2012, **57**, 1191-1334.
10. J.-I. Jung, S. T. Mixture and D. D. Edwards, *Solid State Ionics*, 2010, **181**, 1287-1293.
11. J. Pena-Martinez, D. Marrero-Lopez, J. C. Ruiz-Morales, P. Nunez, C. Sanchez-Bautista, A. J. Dos Santos-Garcia and J. Canales-Vazquez, *Int. J. Hydrogen Energy*, 2009, **34**, 9486-9495.
12. Z. P. Shao and S. M. Haile, *Nature (London, U. K.)*, 2004, **431**, 170-173.
13. A. Yan, M. Yang, Z. Hou, Y. Dong and M. Cheng, *J. Power Sources*, 2008, **185**, 76-84.
14. P. K. Nayak, J. Yang, J. Kim, S. Chung, J. Jeong, C. Lee and Y. Hong, *J. Phys. D: Appl. Phys.*, 2009, **42**, 035102.
15. H. Agura, A. Suzuki, T. Matsushita, T. Aoki and M. Okuda, *Thin Solid Films*, 2003, **445**, 263-267.
16. R. E. Treharne, K. Hutchings, D. A. Lamb, S. J. C. Irvine, D. Lane and K. Durose, *J. Phys. D: Appl. Phys.*, 2012, **45**, 335102.
17. R. J. Cava, A. W. Hewat, E. A. Hewat, B. Batlogg, M. Marezio, K. M. Rabe, J. J. Krajewski, W. F. Peck Jr and L. W. Rupp Jr, *Physica C (Amsterdam, Neth.)*, 1990, **165**, 419-433.
18. P. Karen, E. Suard and F. Fauth, *Inorg. Chem.*, 2005, **44**, 8170-8172.
19. Q. Z. Huang, V. L. Karen, A. Santoro, A. Kjekshus, J. Lindén, T. Pietari and P. Karen, *J. Solid State Chem.*, 2003, **172**, 73-80.
20. P. Karen and A. Kjekshus, *J. Solid State Chem.*, 1994, **112**, 73-77.
21. P. Karen, A. Kjekshus, Q. Huang, V. L. Karen, J. W. Lynn, N. Rosov, I. Natali Sora and A. Santoro, *J. Solid State Chem.*, 2003, **174**, 87-95.
22. I. Felner, I. Nowik, U. Yaron, O. Cohen, E. R. Bauminger, T. Kroener and G. Czjzek, *Phys. Rev. B*, 1993, **48**, 16040-16046.
23. Q. Huang, P. Karen, V. L. Karen, A. Kjekshus, J. W. Lynn, A. D. Mighell, N. Rosov and A. Santoro, *Phys. Rev. B*, 1992, **45**, 9611-9619.
24. A. L. Shaula, Y. V. Pivak, J. C. Waerenborgh, P. Gaczyński, A. A. Yaremchenko and V. V. Kharton, *Solid State Ionics*, 2006, **177**, 2923-2930.
25. A. Demont, M. S. Dyer, R. Sayers, M. F. Thomas, M. Tsiamtsouri, H. N. Niu, G. R. Darling, A. Daoud-Aladine, J. B. Claridge and M. J. Rosseinsky, *Chem. Mater.*, 2010, **22**, 6598-6615.
26. F. Ramezanipour, J. E. Greedan, L. M. D. Cranswick, V. O. Garlea, R. L. Donaberger and J. Siewenie, *J. Am. Chem. Soc.*, 2012, **134**, 3215-3227.
27. F. Ramezanipour, B. Cowie, S. Derakhshan, J. E. Greedan and L. M. D. Cranswick, *J. Solid State Chem.*, 2009, **182**, 153-159.
28. F. Millange, E. Suard, V. Caignaert and B. Raveau, *Mater. Res. Bull.*, 1999, **34**, 1-9.
29. G. Hautier, C. Fischer, V. Ehrlacher, A. Jain and G. Ceder, *Inorg. Chem.*, 2011, **50**, 656-663.
30. R. Grau-Crespo, S. Hamad, C. R. A. Catlow and N. H. de Leeuw, *J. Phys.: Condens. Matter*, 2007, **19**, 256201.
31. B. J. Morgan and G. W. Watson, *J. Phys. Chem. Lett.*, 2011, **2**, 1657-1661.
32. S. Benny, R. Grau-Crespo and N. H. de Leeuw, *Phys. Chem. Chem. Phys.*, 2009, **11**, 808-815.
33. J. J. Adkin and M. A. Hayward, *J. Solid State Chem.*, 2006, **179**, 70-76.
34. Q. Wang, R. Grau-Crespo and N. H. de Leeuw, *J. Phys. Chem. B*, 2011, **115**, 13854-13861.

35. Q. Wang and N. H. de Leeuw, *Mineral. Mag.*, 2008, **72**, 525-529.
36. Y. Seminovski, P. Palacios, P. Wahnnon and R. Grau-Crespo, *Appl. Phys. Lett.*, 2012, **100**, 102112.
37. D. O. Scanlon and A. Walsh, *Appl. Phys. Lett.*, 2012, **100**, 251911.
38. B. Saha, J. Acharya, T. D. Sands and U. V. Waghmare, *J. Appl. Phys.*, 2010, **107**, 033715.
39. D. J. Fredeman, P. H. Tobash, M. A. Torrez, J. D. Thompson, E. D. Bauer, F. Ronning, W. W. Tipton, S. P. Rudin and R. G. Hennig, *Phys. Rev. B*, 2011, **83**, 224102.
40. M. Pishahang, C. E. Mohn, S. Stolen and E. Bakken, *RSC Adv.*, 2012, **2**, 10667-10672.
41. Y. L. Lee, J. Kleis, J. Rossmeisl and D. Morgan, *Phys. Rev. B*, 2009, **80**, 224101.
42. M. Regulski, R. Przeniosło, I. Sosnowska, D. Hohlwein and R. Schneider, *J. Alloys Compd.*, 2004, **362**, 236-240.
43. D. Rodic, V. Spasojevic, V. Kusigerski, R. Tellgren and H. Rundlof, *Phys. Status Solidi B*, 2000, **218**, 527-536.
44. M. Catti, G. Valerio and R. Dovesi, *Phys. Rev. B*, 1995, **51**, 7441-7450.
45. M. Faucher and J. Pannetier, *Acta Crystallogr., Sect. B: Struct. Sci.*, 1980, **36**, 3209-3211.
46. L. G. Liu, *J. Appl. Phys.*, 1971, **42**, 3702-3704.
47. W. L. Roth, *J. Phys. Chem. Solids*, 1964, **25**, 1-10.
48. R. Miloua, F. Miloua, A. Arbaoui, Z. Kebbab and N. Benramdane, *Solid State Commun.*, 2007, **144**, 5-9.
49. I. Felner and J. Gersten, *Czech J. Phys.*, 1996, **46**, 1421-1422.
50. D. A. Kudryavtsev, B. V. Mill, N. F. Vedernikov and I. S. Shaplygin, *Inorg. Mater.*, 1992, **28**, 943-946.
51. D. DuBoulay, E. N. Maslen, V. A. Streltsov and N. Ishizawa, *Acta Crystallogr., Sect. B: Struct. Sci.*, 1995, **51**, 921-929.
52. L. Miranda, K. Boulahya, A. Varela, J. M. Gonzalez-Calbet, M. Parras, M. Hernando, M. T. Fernandez-Diaz, A. Feteira and D. C. Sinclair, *Chem. Mater.*, 2007, **19**, 3425-3432.
53. H. T. Stokes and D. M. Hatch, *J. Appl. Crystallogr.*, 2005, **38**, 237-238.
54. J. Cui, Q. Huang and B. H. Toby, *Powder Diffr.*, 2006, **21**, 71-79.
55. V. F. Sears, *Neutron News*, 1992, **3**, 26-37.
56. P. M. Woodward and P. Karen, *Inorg. Chem.*, 2003, **42**, 1121-1129.
57. W. H. Baur, *Acta Crystallogr., Sect. B: Struct. Sci.*, 1974, **30**, 1195-1215.
58. K. Momma and F. Izumi, *J. Appl. Crystallogr.*, 2011, **44**, 1272-1276.
59. H. Saalfeld, *Z. Kristallogr.*, 1964, **120**, 342-348.
60. A. Munoz, J. A. Alonso, M. J. Martinez-Lope and J. L. Martinez, *Chem. Mater.*, 2004, **16**, 4087-4094.
61. N. Kallel, S. Ben Abdelkhalek, S. Kallel, O. Pena and M. Oumezzine, *J. Alloys Compd.*, 2010, **501**, 30-36.
62. J. H. Shin, M. S. Song and J. Y. Lee, *J. Electroceram.*, 2006, **17**, 205-209.
63. E. García-Matres, J. L. Martínez, J. Rodríguez-Carvajal, J. A. Alonso, A. Salinas-Sánchez and R. Saez-Puche, *J. Solid State Chem.*, 1993, **103**, 322-333.
64. G. Kresse and D. Joubert, *Phys. Rev. B*, 1999, **59**, 1758-1775.
65. G. Kresse and J. Furthmüller, *Phys. Rev. B*, 1996, **54**, 11169-11186.
66. J. P. Perdew, K. Burke and M. Ernzerhof, *Phys. Rev. Lett.*, 1996, **77**, 3865-3868.
67. S. L. Dudarev, G. A. Botton, S. Y. Savrasov, C. J. Humphreys and A. P. Sutton, *Phys. Rev. B*, 1998, **57**, 1505-1509
68. PANalytical B. V., *X'Pert HighScore Plus*, Almelo, The Netherlands, 2006.
69. International Center for Diffraction Data, *Powder Diffraction File PDF-2*, Pennsylvania, U.S.A., 2007.
70. A. A. Coelho, *J. Appl. Crystallogr.*, 2003, **36**, 86-95.
71. A. A. Coelho, *TOPAS Academic: General Profile and Structure Analysis Software for Powder Diffraction Data, Version 4.1*, Bruker AXS, Karlsruhe, Germany, 2007.

72. B. H. Toby, *J. Appl. Crystallogr.*, 2001, **34**, 210-213.
73. A. C. Larson and R. B. Von Dreele, *General Structure Analysis System (GSAS)*, 1994.